Geophysical Journal International

Geophys. J. Int. (2019) **218,** 401–413
Advance Access publication 2019 March 27
GJI Geodynamics and tectonics

doi: 10.1093/gji/ggz158

Some remarks on Glacial Isostatic Adjustment modelling uncertainties

D. Melini[1] and G. Spada[2]

[1] *Istituto Nazionale di Geofisica e Vulcanologia, Sezione di Sismologia e Tettonofisica, 00143 Roma, Italy*
[2] *Dipartimento di Scienze Pure e Applicate (DiSPeA), Università di Urbino Carlo Bo, Via Santa Chiara, 27, 61029 Urbino, Italy.*
E-mail: giorgio.spada@gmail.com

Accepted 2019 March 25. Received 2019 March 21; in original form 2018 September 17

SUMMARY

Glacial Isostatic Adjustment (GIA) modelling has recently seen a significant development, stimulated by the need of understanding past, current and future sea level variations and geodetic signals associated with climate change. Our main motivation is that albeit its importance is well recognized within the climate science community, the problem of classifying and quantifying GIA modelling uncertainties has so far received little attention. Here, we consider two possible ways of defining and evaluating these uncertainties. The first is associated with limited knowledge of input model parameters (e.g. the viscosity profile of the Earth's mantle or the deglaciation history), once it is assumed that the ice margins are known and a unique set of relative sea level (RSL) data are used to constrain the model. We also discuss a second and more problematic source of uncertainty, associated with structural differences in GIA models, stemming from distinct eustatic curves and ice margins geometries, different RSL constraints, non-identical input parameters and different numerical solution schemes. By analysing the present-day 'GIA fingerprints' of relative and absolute sea level change, and exploring the GIA contribution to secular sea level rise and to the time-variations of the Earth's gravity field, here we evaluate the two types of uncertainty showing that they are (i) of significant amplitude and (ii) of comparable importance.

Key words: Loading of the Earth; Sea level change; Time variable gravity.

1 INTRODUCTION

The interpretation of various geophysical data, including sea level rise observations, gravity field variations from satellite missions and ground-based geodetic observations requires evaluating the contribution associated with the ongoing Glacial Isostatic Adjustment (GIA) in response to the melting of the late-Pleistocene ice sheets (see Whitehouse 2009; Spada 2017; Whitehouse 2018, for a review). Solving the 'sea level equation' (hereinafter referred to as SLE, see Farrell & Clark 1976), the present spatial variability of various geodetic quantities associated with GIA can be predicted and visualized. In symbolic form, the SLE reads

$$S(\omega, t) = N - U, \tag{1}$$

where $\omega = (\theta, \lambda)$, θ and λ are the colatitude and the longitude, respectively, and t is the time. In this study, our main focus is on changes in present-day relative and absolute sea level (S and N, respectively), but we will also consider vertical land motion (VLM, U), and variations in the gravity potential Φ associated with GIA (e.g. Tamisiea 2011; Spada 2017; Whitehouse 2018).

The patterns of fields S, N and U, first dubbed GIA 'fingerprints' by Plag & Jüettner (2001), are sensitive to the details of the Earth's viscoelastic profile and of the melting chronology of the ice sheets, which are not perfectly known *a priori* (e.g. Lambeck *et al.* 2014). More uncertainties may arise from different numerical implementations of the SLE within different research groups and possible methodological discordances (e.g. Purcell *et al.* 2016; Peltier *et al.* 2018). Although significant efforts have been made (Spada *et al.* 2011) and are in progress (Martinec *et al.* 2018), the GIA community has not yet produced an agreed set of 'gravitationally' and 'topographically self-consistent' solutions of the SLE (Peltier 1994), which would certainly mitigate modelling uncertainties. Furthermore, since the models are progressively improved as new observational constraints are obtained from space-borne or ground-based geodetic instrumentations (e.g. King *et al.* 2010), GIA corrections are not given once and for all. Although this is often overlooked, 'exact' GIA corrections are not possible (Tamisiea 2011; Spada 2017).

Because of the inherent complexity of GIA modelling (see e.g. Lambeck *et al.* 2003; Mitrovica & Milne 2003; Martinec *et al.* 2018) defining, identifying and weighing all possible sources of uncertainty is not straightforward (Kennedy & O'Hagan 2001; Sørensen *et al.* 2001). Furthermore, being the GIA response markedly regional, the uncertainties may have different amplitudes and origins

at different spatiotemporal scales. Globally, since the long-term trend of relative sea level (RSL) at tide gauges (TGs) is significantly affected by GIA (Spada & Galassi 2012; Jevrejeva *et al.* 2014; Hay *et al.* 2015), uncertainties in GIA corrections represent a major challenge in the assessment of present mean sea level rise (Wöppelmann & Marcos 2016). Furthermore, quantifying the GIA modelling uncertainty is of fundamental importance in order to establish the recent sea level budget (WCRP 2018). In some previous studies, uncertainties on the imprints of GIA have been estimated by varying the Earth's viscosity profile and the lithospheric thickness within a plausible range, both in global (e.g. Tamisiea 2011; Hay *et al.* 2015; Pfeffer *et al.* 2017; Santamaría-Gómez *et al.* 2017) and in regional contexts (e.g. Stocchi & Spada 2009; Serpelloni *et al.* 2013; Vacchi *et al.* 2016). This approach is useful to test the sensitivity of GIA predictions to the Earth's rheology, but it is recognized that keeping the ice sheets time-histories unaltered may introduce large variations in the GIA estimates (e.g. Tamisiea 2011) and, consequently, it may deteriorate the fit with the global RSL data constraining the model.

In a recent paper, Caron *et al.* (2018) have studied the GIA modelling uncertainty using Bayesian methodologies, with the purpose of providing rigorous corrections to trends in surface mass from the Gravity Recovery and Climate Experiment (GRACE) satellite. In their analysis, Caron *et al.* (2018) tested a population of $\sim 10^5$ GIA models characterized by different rheological profiles and melting histories, using RSL data as constraints. However, they have mainly focused on the gravity field variation due to GIA, without addressing the problem of finding the GIA uncertainty on secular sea level rise, which is the main purpose of our work. Recent efforts to better constrain the GIA fingerprints uncertainty, such as that of Caron *et al.* (2018) and this study, are also stimulated by existing heuristic estimates that can be certainly improved, such as the ± 20 per cent rule proposed in the context of GRACE[1].

The paper is organized as follows. In Section 2, we define and describe in detail the two types of uncertainty considered in this study (uncertainty of type T1, associated with limited knowledge of input parameters and T2, associated with structural differences in GIA models). Section 3 describes the ensemble modelling approach that we have set up to define the T1 uncertainty, and in Section 4 we study the T1 uncertainties on predictions of Holocene RSL variations. In Section 5, we analyse the T1 uncertainties on some of the present-day imprints of GIA and we consider their effect on the assessment of secular sea level rise, while in Section 6 we discuss the T2 uncertainty. Our conclusions are drawn in Section 7.

2 UNCERTAINTIES IN GIA MODELLING

With the purpose of characterizing and estimating uncertainties in the GIA fingerprints, next we distinguish between two different types of uncertainty, both ultimately arising from the fact that every model is a simplification of reality. In doing so, we adopt the methodological approach suggested by Sørensen *et al.* (2001) in a different context; a more general view about the uncertainties associated with modelling is given by Kennedy & O'Hagan (2001). Although the elastic response of the Earth to the melting of present-day glaciers and ice sheets is also governed by the SLE (e.g. Spada 2017), here we only consider the contribution to GIA from the late-Pleistocene ice sheets since this is sensitive to the Earth's viscosity profile, which indeed represents a major source of uncertainty.

Uncertainties of the first type (T1), or 'input uncertainties', only stem from internal factors and reflect imperfect knowledge about basic parameters of the GIA model (*i.e.* the chosen Earth viscosity profile and the melting history of individual ice sheets). These quantities are generally constrained by imposing the agreement of model predictions with RSL data from sites across ice-covered areas at the Last Glacial Maximum (LGM). Here, the T1 uncertainties are estimated by a Monte Carlo simulation in which the performance of a large ensemble of GIA models is tested against RSL data extracted from the unique global database presently accessible[2], published by Tushingham & Peltier (1993). Although high-quality RSL observations are available from specific regions (see e.g. Lambeck *et al.* 1998; Engelhart *et al.* 2011; Lambeck *et al.* 2014; Steffen *et al.* 2014; Simon *et al.* 2016) we believe that despite its age and possible limitations, the Tushingham and Peltier's database is a fair starting point to get a general estimate of T1 uncertainty, both in terms of pattern and amplitude. Furthermore, this same database has been originally used to constrain the GIA model ICE-3G, which is used here to illustrate how the T1 uncertainty can be estimated. Of course, we are aware that this choice could alter the spatial pattern of T1 uncertainties, and the locations where they exceed the RSL data uncertainty.

In our analysis, each GIA model represents a possible realization of ICE-3G (Tushingham & Peltier 1991, 1992), in which the original viscosity profile VM1 and the spatial distribution of the ice sheets volumes are simultaneously varied scaling the local ice thickness by a random factor. However, the history of total ice volume is kept unaltered since it is constrained by sea level observations far from the former ice sheets (Tushingham & Peltier 1991). An evaluation of T1 uncertainties is also possible for other more recent global GIA models, structurally more complex than ICE-3G(VM1). However, an exhaustive Monte Carlo simulation would be more challenging for these GIA models, which account for the migration of shorelines, the transition between floating and grounded ice (or *vice versa*), and rotational effects. In fact, including these features in modelling demands two nested iterations of the SLE (see e.g. Mitrovica & Milne 2003; Spada & Galassi 2017), which require significant computing resources. Furthermore, the detailed spatiotemporal description of these recent GIA models would demand a higher resolution, which would further increase the computational burden. Hence, to evaluate the T1 uncertainty, for the time being we maintain the relatively simple ICE-3G(VM1) model to reduce the numerical complexity of the underlying SLE. By this approach, we expect to identify at least the major sources of modelling uncertainties and their impact on GIA.

At least another type of uncertainty exists; this structural uncertainty, which is more problematic to quantify than T1 (Sørensen *et al.* 2001) and is not independent on it, is referred to as T2 uncertainty. Here, T2 is attributed to various external and internal factors. These include (but are not limited to) differences in the solution methods of the SLE in use by different research groups, the adoption of different eustatic curves based on RSL observations in the far-field of the former ice sheets, the utilization of qualitatively and/or quantitatively different sets of external geophysical constraints (e.g. the location of paleo-shorelines or present-day

[1] See https://grace.jpl.nasa.gov/data/get-data/gia-trends/ (last visited 2019 March 15).

[2] See ftp://ftp.ncdc.noaa.gov/pub/data/paleo/paleocean/relative_sea_level/ (last visited on 2018 December 19).

geodetic observations), or diverging *a priori* assumptions about the input Earth's rheological profile. Here, the T2 uncertainty on the geodetic fingerprints and on secular sea level rise is estimated by considering a mini-ensemble composed by two state-of-the-art, independently developed models that are characterized by significant structural differences. This same approach, but limited to the relative sea level fingerprints, has been adopted by the IPCC AR5 (Church *et al.* 2013). Since the paucity of global GIA models presently available certainly hinders a precise estimate of T2, our results will be certainly reconsidered and refined in the future. It should also be remarked that, at least currently, the limit between T1 and T2 can be blurred because imperfect knowledge on GIA parameters (e.g. the viscosity profile of the mantle) reflects whatever information is contained in the data, and the choice of a data set belongs to T2 uncertainty. As computer power evolves, it is possible that through a more systematic exploration of the ice margins history and of the rheological profiles, more and more uncertainty that is currently of type T2 will be transferred into T1; for example, it will be easily possible to construct a large ensemble of GIA models with time-evolving shorelines in which the ice sheets distribution and the Earth's viscosity profile are randomized. In this respect, a significant step forward has been recently made by Caron *et al.* (2018) using a large ensemble of GIA models constrained by an RSL data set using Bayesian methodologies. Their approach, however, differs from ours since no distinction is made between possible different 'types' of uncertainty, and the problem of finding the GIA uncertainty on the amount of secular sea level rise, which is central to this study, has not been addressed.

3 ENSEMBLE GIA MODELLING

To estimate the T1 uncertainty, we have adopted a straightforward Monte Carlo approach, in which a large number (5×10^5) of random variants of the nominal ICE-3G(VM1) model (Tushingham & Peltier 1991, 1992) are generated, which differ from it by the value of some key input parameters. Adopting the same ice sheets margins as in ICE-3G(VM1), we randomize the ice topography by rescaling the local ice thickness by a few scaling factors to avoid a completely random ice distribution, possibly characterized by islands and troughs in ice sheets. In the random ice models, the volumes of the two major ice sheets in the Northern Hemisphere (*i.e.* Laurentide and Fennoscandia) are rescaled by a random, time-independent factor (the thickness of the Greenland ice sheet is rescaled according to that of Laurentide). However, the volume of the Antarctica ice sheet is rescaled by a time-dependent factor in order to maintain the history of total ice volume unaltered; such time-history is indeed constrained by sea level observations in the equatorial ocean (Tushingham & Peltier 1991). Using this parametrization for the ice sheets melting histories, we can introduce some variability in the spatial distribution of ice masses using a minimum number of free parameters (two). A similar parametrization has been adopted by Caron *et al.* (2018), who defined six constant regional ice scaling coefficients. Furthermore, for each element of the ensemble, we have randomly chosen new values of lithospheric thickness and mantle viscosity within a range including ICE-3G(VM1) values (see Table 1), maintaining the same structure (*i.e.* the thickness of mantle layers, the values of density and of shear moduli) of the nominal model. All models of the ensemble are self-gravitating and characterized by an incompressible linear Maxwell viscoelastic rheology (see e.g. Wu & Peltier 1982; Spada *et al.* 2011).

To extract a subset of statistically equivalent GIA models from the ensemble, we have used the constraints provided by the Holocene RSL observations of the Tushingham & Peltier (1993) database, which were originally adopted to construct the nominal ICE-3G(VM1) model. The locations of the sites of the database are shown in Fig. 1. In particular, for each model in the ensemble, we have computed a numerical solution of the SLE (eq. 1) by means of the open source program SELEN (Spada & Stocchi 2007), assuming fixed shorelines, no transition between grounded and floating ice, and no rotational feedback, *i.e.* we have followed the classical formulation of the SLE given by Farrell & Clark (1976). These assumptions, coherent with those adopted in the development of ICE-3G(VM1), will be relaxed in the estimation of T2 uncertainty. For each member of the ensemble, we have obtained synthetic Holocene RSL curves at all the 191 sites in the Tushingham & Peltier (1993) database inside the ice sheets margins (see the white circles in Fig. 1) and, exactly following Tushingham & Peltier (1991), we have computed the global measure of the misfit, or 'variance':

$$\sigma_{\mathrm{RSL}} = \frac{1}{N_{\mathrm{obs}}} \sqrt{\sum_{i,t} \left[\mathrm{RSL}_i^{\mathrm{pre}}(t) - \mathrm{RSL}_i^{\mathrm{obs}}(t)\right]^2}, \tag{2}$$

where $N_{\mathrm{obs}} = 1{,}019$ is the number of RSL observations, $\mathrm{RSL}_i^{\mathrm{pre}}(t)$ and $\mathrm{RSL}_i^{\mathrm{obs}}(t)$ are the predicted and observed RSL at time t for the i-th site ($i = 1, \ldots, N_{\mathrm{RSL}} = 191$), respectively. Following Tushingham & Peltier (1991), we account for the uncertainty Δt_{obs} in the observation age t_{obs} by evaluating GIA predictions at the three times $t = t_{\mathrm{obs}}$ and $t = t_{\mathrm{obs}} \pm \Delta t_{\mathrm{obs}}$ and choosing, for the evaluation of σ_{RSL}, the t value minimizing $|\mathrm{RSL}_i^{\mathrm{pre}}(t) - \mathrm{RSL}_i^{\mathrm{obs}}(t)|$. The ensemble models that are statistically equivalent have been singled out by comparing their σ_{RSL} with that obtained adopting the nominal ICE-3G(VM1); see Table 1. By a Fisher F-test (e.g. Kotz *et al.* 2004), it turns out that 23,709 (*i.e.* 4.6 per cent) of the 5×10^5 models in the ensemble are statistically undistinguishable from the nominal ICE-3G(VM1) at the 95 per cent confidence level. Table 1 lists, for each input parameter, the average and standard deviation computed over the ensemble of models that are equivalent to ICE-3G(VM1). The reported values show a strong sensitivity of σ_{RSL} to mantle viscosities and a less marked sensitivity to lithospheric thickness. Conversely, the dependence of σ_{RSL} on the ice sheet rescaling factors is weak since the corresponding averages and standard deviations are close to those expected for a uniform distribution. For all input parameters, the ICE-3G(VM1) nominal values fall within the 1σ ensemble confidence intervals.

4 HOLOCENE SEA LEVEL CHANGE

In Fig. 1, the small dots show the location of all the 392 sites of the Tushingham & Peltier (1993) RSL database. For a selection of them, depicted in colours, Fig. 2 shows RSL data with error bars, modelling predictions and T1 uncertainties. To underline the geographical pattern of the T1 uncertainty on RSL, we have selected a few sites for which the number of RSL observations available in the database is relatively large, and located in Canada (Fig. 2a), Northern Europe (Fig. 2b) and in low-latitude locations in the far-field of the former ice sheets (Fig. 2c). In Fig. 2(d), we consider the only four sites available for Antarctica in the RSL database. Fig. 1 clearly shows that the density of points on the East coast of the US or on the British Isles is measurably greater than around the coast of Antarctica. It is also clear that the data are more concentrated in the Northern Hemisphere than in the Southern Hemisphere, due to the distribution of the landmasses. A similar observation can be made

Table 1. Input parameters considered in the GIA ensemble modelling. For each parameter, we list the explored range, the nominal ICE-3G(VM1) value and the average and standard deviation computed over the models that reproduce RSL observations equivalently to ICE-3G.

Input parameter	Range	Nominal value for ICE-3G(VM1)	Ensemble T1 average and standard deviation
Lithospheric thickness (km)	90–150	120	110 ± 13
Upper-mantle viscosity (10^{21} Pa s)	0.5–3.5	1	1.5 ± 0.5
Lower mantle viscosity (10^{21} Pa s)	1–20	2	2.1 ± 0.6
Scale factor for Laurentide	0.8–1.2	1.0	1.0 ± 0.1
Scale factor for Fennoscandia	0.8–1.2	1.0	1.0 ± 0.1

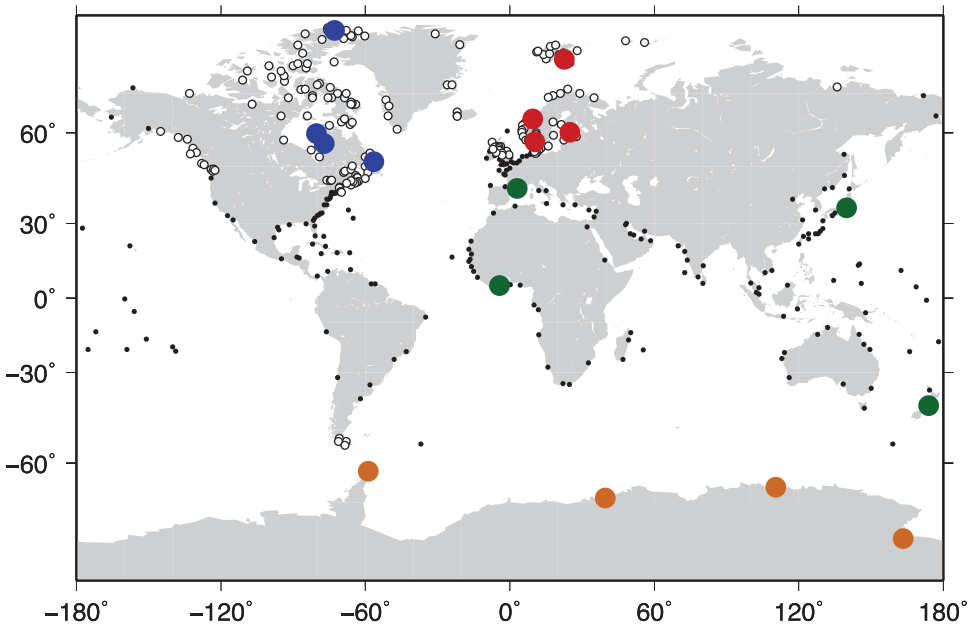

Figure 1. Coloured dots mark the sites from the Tushingham & Peltier (1993) database for which we show RSL curves and GIA uncertainties in Fig. 2 (blue, red and orange dots mark sites located in North America, Northern Europe and Antarctica, respectively, while green dots show sites located in the far-field of the former ice sheets). Small black dots mark the locations of all the 392 sites in the database, white ones indicate the 191 sites that have been employed to compute the ensemble variance using eq. (2).

about the temporal distribution of the data in the Tushingham & Peltier (1993) RSL database, with comparatively more RSL records being available for the Holocene than for epochs close to the LGM. The limited information content in the RSL data clearly hinders a detailed mapping of the global pattern of GIA uncertainties. The use of updated RSL data sets, such as the compilation of Caron *et al.* (2017) or the combined RSL and geodetic data set utilized by Caron *et al.* (2018), would certainly mitigate the intrinsic limitations imposed by the old data set considered here. In order to avoid biases associated with the spatiotemporal distribution of the data, improved cost functions should be constructed, while in our variance computation each data point is taken as *a priori* equally valuable (see eq. 2 above). This, however, falls outside the scope of our exercise, which is aimed at the determination of the T1 GIA uncertainties specifically associated with model ICE-3G, for which the use of the Tushingham & Peltier (1993) database and of the statistics originally employed is in order. Nevertheless, we recognize that the assessment of potential biases due to RSL data spatiotemporal distribution is of paramount importance to correctly estimate GIA model uncertainties, and should hopefully be the subject of future investigations.

The solid lines in Fig. 2 show the RSL curves obtained for the nominal ICE-3G(VM1). The 1σ confidence intervals, shaded in colours, indicate the T1 uncertainty of each RSL curve. The intervals are evaluated by computing the standard deviation on the ensemble of 23,709 GIA models that are statistically undistinguishable from the nominal ICE-3G(VM1), according to the definition given in Section 3. For sites located beneath or in the neighbours of the former ice sheets Fig. 2(a) and (b), the GIA uncertainties are significant, and sometimes exceed the intrinsic uncertainty of RSL data. Furthermore, GIA uncertainties show generally a tendency to increase with age BP since varying the Earth's viscosity profile has a relatively minor effect for relatively short times. Conversely, in far-field sites such as in Fig. 2(c), the GIA uncertainties never exceed the data uncertainties. Indeed, for these sites the time evolution of RSL is known to be mostly sensitive to the history of the total volume of the ice sheets (Tushingham & Peltier 1992), which is the same for all the models in the ensemble. A large GIA uncertainty is noteworthy along the margins of Antarctica Fig. 2(d), although the general trend of the data is reasonably well matched.

The whole Tushingham & Peltier (1993) database contains data for 392 RSL sites (their distribution is shown in Fig. 1). With further computations, not shown here, we estimated the T1 uncertainty on RSL predictions, $\sigma_{\mathrm{RSL}^{\mathrm{pre}}}$, for each data point in the database and obtained the corresponding relative uncertainty as the ratio

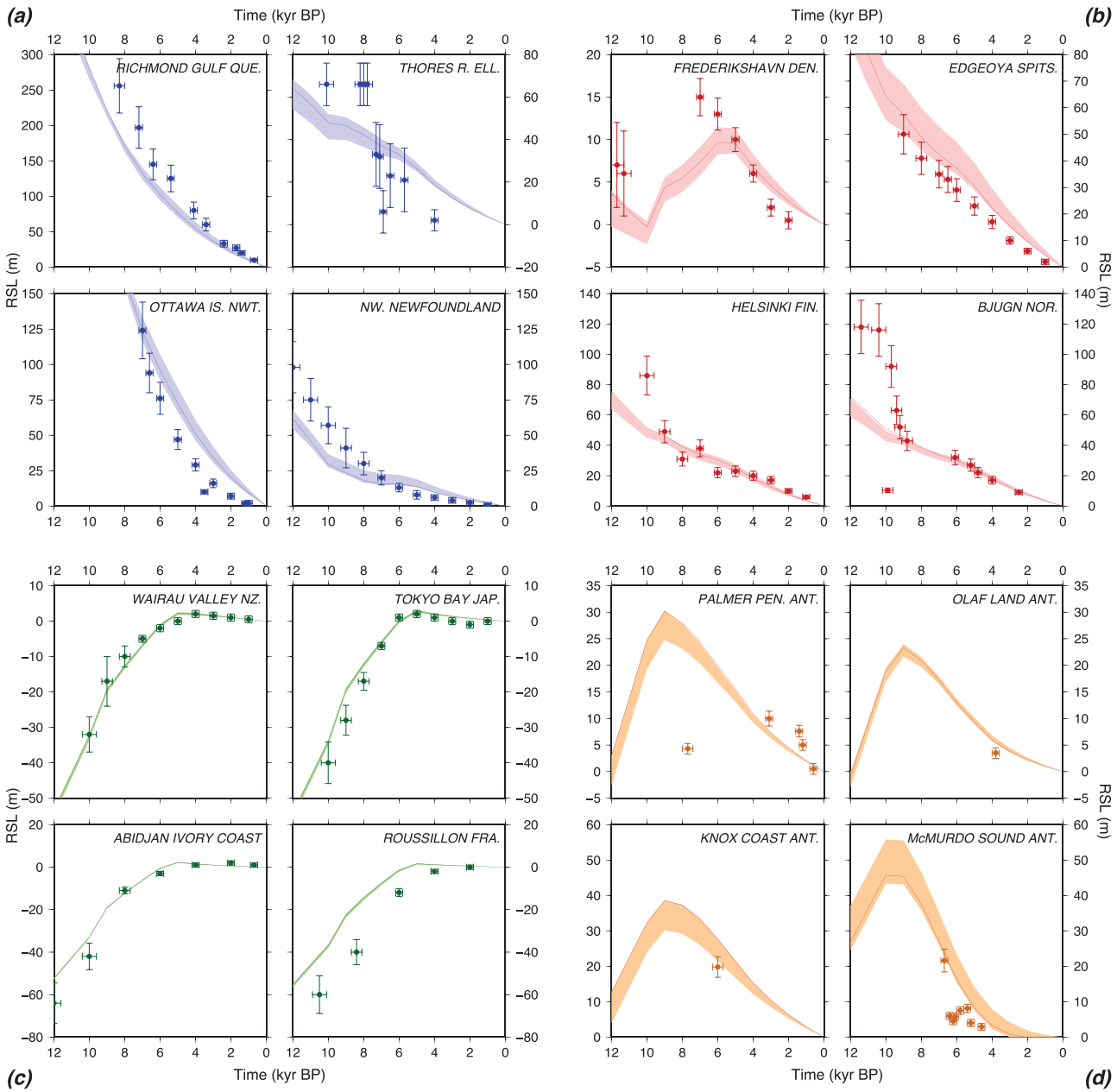

Figure 2. RSL data from the Tushingham & Peltier (1993) database (circles with error bars) compared with synthetic nominal RSL curves for ICE-3G(VM1), represented by solid lines, and their 1σ GIA modelling uncertainties T1, represented by shaded regions. Sites located in North America (a), in Northern Europe (b), in the low-latitude oceanic region (c) and in Antarctica (d) are identified by different colours. The location of the selected sites is shown in Fig. 1.

$|\sigma_{\mathrm{RSL}^{\mathrm{pre}}}/\mathrm{RSL}^{\mathrm{pre}}|$. We have found that the maximum GIA relative uncertainties are attained at ∼7 kyr BP, and that relative uncertainties are larger in the vicinity of formerly glaciated regions, confirming the spatial pattern suggested by the few sites shown in Fig. 2. Considering the whole Tushingham & Peltier (1993) database, we have found that 20 per cent of the GIA RSL predictions have a relative T1 uncertainty exceeding 30 per cent.

5 PRESENT-DAY GIA

In previous sections, we have determined a set of statistically equivalent GIA models by comparing their outputs against Holocene RSL data. Here, these same models are utilized to estimate the T1 GIA uncertainties on a suite of present-day geodetic quantities. This is important to better quantify the influence of GIA on variations in the climate system, which are now detected by a range of different observation methods, such as relative sea level change at individual TGs, secular sea level rise, absolute sea level variations and gravity changes.

5.1 Relative sea level fingerprint and GIA corrections at tide gauges

For the nominal model ICE-3G(VM1), the pattern of the rate of present-day relative sea level change $\dot{S}$ is shown in Fig. 3(a). The map illustrates the well-known features described by Mitrovica & Milne (2002), that is, the sea level fall associated with post-glacial rebound in the previously ice-covered polar regions, the rise across

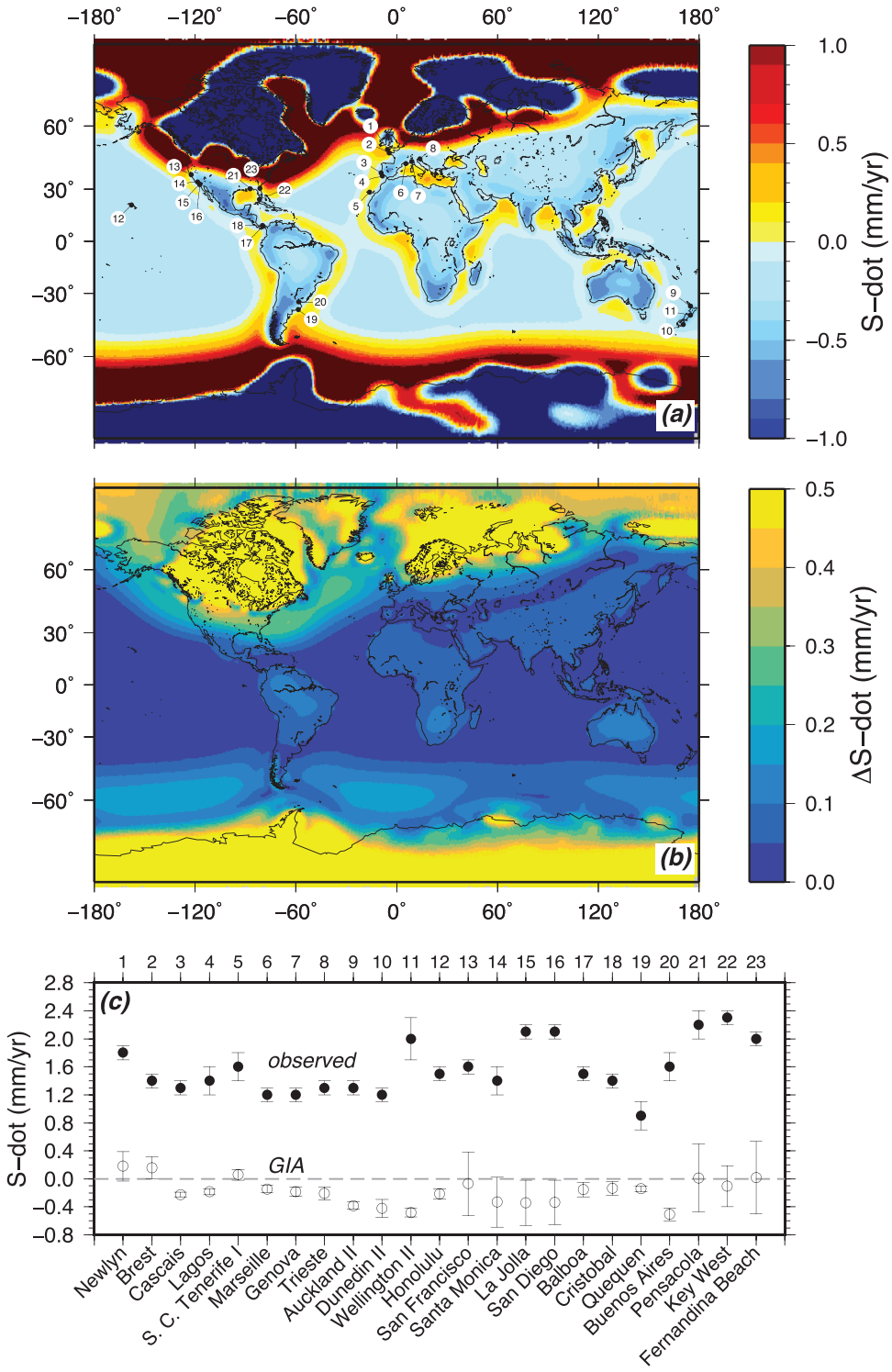

Figure 3. $\dot{S}$ fingerprint for the nominal ICE-3G(VM1) model (a) and its T1 1σ uncertainty $\Delta\dot{S}$ (b). The circles in (a) show the 23 TG sites of Douglas (1997). Observed $\dot{S}$ at TGs (filled circles) and the corresponding GIA corrections (open circles) are shown in (c). For ease of viewing, the uncertainties shown in (c) correspond to 2σ, while the colour scales in (a) and (b) are saturated.

the collapsing forebulges, the broad fall associated with 'equatorial ocean syphoning' and the offshore sea level rise associated with 'continental levering'. Since the Farrell & Clark (1976) theory that we employ here does not account for the rotational feedback on sea level (Milne & Mitrovica 1998), the characteristic long-wavelength harmonic degree $l = 2$ and order $m = 1$ pattern (e.g. Spada 2017) does not appear on the map. Furthermore, since here we assume fixed shorelines and in ICE-3G(VM1) the melting ceased ∼4000 yr ago, the fingerprint shown has the property

$$\langle \dot{S}(\omega) \rangle = 0, \tag{3}$$

where the dot indicates the time derivative evaluated at present time, and $\langle\cdots\rangle$ denotes the ocean-average (see e.g. Tamisiea 2011). Eq. (3) manifests the fact that presently GIA is not causing a net variation in the mass of the oceans, but only regional variations in the rate of change of RSL. The spatial distribution of the 1σ T1 uncertainty ($\Delta\dot{S}$), shown in Fig. 3(b), is minimum ($\leq$0.1 mm yr^{-1}) in the equatorial region and at mid-latitudes, but it increases to values as large as $\sim$2.2 mm yr^{-1} across the formerly glaciated regions and the surrounding collapsing forebulges. Relatively high values of $\Delta\dot{S}$ in the polar regions that were covered by thick ice reflect an enhanced sensitivity to variations in the Earth's viscosity profile, compared to low-latitude locations (e.g. Tushingham & Peltier 1991). Visually, $\Delta\dot{S}$ roughly scales with $|\dot{S}|$; as a rule of thumb we find $\Delta\dot{S}/|\dot{S}| \approx 0.2$.

GIA corrections to rates of sea level change observed at TGs are essential for the assessment of secular sea level rise (Mitrovica *et al.* 2001; Spada & Galassi 2012; Jevrejeva *et al.* 2014; Wöppelmann & Marcos 2016). From Fig. 3(a), we have obtained GIA corrections at the 23 high-quality TGs considered by Douglas (1997) in his redetermination of global mean sea level rise (GMSLR); similarly, their 1σ T1 uncertainties are obtained from Fig. 3(b). In Fig. 3(c), the GIA corrections at TGs (bottom, the open symbols) are compared with the rates observed during last century, obtained by linear regression (Spada & Galassi 2012) from Permanent Service for Mean Sea Level yearly records (see PSMSL 2013). It is apparent that the uncertainties on the observed TG rates, which mostly reflect the energetic decadal oscillations of sea level (e.g. Sturges & Hong 2001), often exceed those associated with GIA. Indeed, the Douglas (1997) TGs (the dots in Fig. 3a) are mainly sited beyond the collapsing lateral bulges where generally $\dot{S} < 0$ and $\Delta\dot{S}$ is relatively small. There are, however, notable exceptions, namely the sites along the North American West Coast (sites 13–16, from San Francisco to San Diego) and those in South East North America (21–23, from Pensacola to Fernandina Beach), but a similar pattern is also visible for the English Channel (sites 1–2, Newlyn and Brest). At these sites, the GIA T1 uncertainty exceeds the data error bars. Again, this manifests the sensitivity of the near-field Earth's response to perturbations of the rheological profile.

5.2 Secular sea level rise

Observed trends at TGs along with the GIA ensemble results can be used to estimate the T1 uncertainties on secular GMSLR μ. Historically, μ has been evaluated by correcting the TG trends using a single or a few GIA models, in which the rheological parameters are varied within a plausible range (see Table 1 of Spada & Galassi 2012). Here, we exploit our large ensemble, with the purpose of estimating the effective role of GIA on the uncertainties associated with μ.

Following Spada & Galassi (2012), we compute μ as a simple average

$$\mu = \frac{1}{N_{\rm tg}} \sum_{i=1}^{N_{\rm tg}} r_i, \tag{4}$$

where r_i ($i = 1, \ldots, N_{\rm tg}$) are the rates of secular sea level rise observed at the $N_{\rm tg} = 23$ high-quality TGs considered by Douglas (1997; see Fig. 3c). The values of r_i are taken directly from Table 2 of Spada & Galassi (2012). It should be noted that due to the limited geographical coverage of the employed TGs, the value of μ given by (4) could be biased by an unknown amount. This has been discussed in Spada & Galassi (2012). From their Table 1, it can be noted, however, that more sophisticated averaging methods, such as those based on the empirical orthogonal function technique, lead to values of GMSLR that are comparable, within their uncertainty, with that obtained by a simple average.

As discussed by Spada & Galassi (2012), different measures of uncertainty on the GMSLR have been employed in literature. According to their Table 1, most studies quantify the GMSLR uncertainty either in terms of the root mean square (rms) of individual TG rates, or as a standard deviation of their mean (sdom). The rms is computed as a sample standard deviation:

$$\delta\mu_{\rm rms} = \sqrt{\frac{\sum_{i=1}^{N_{\rm tg}} (r_i - \mu)^2}{N_{\rm tg} - 1}}, \tag{5}$$

while the sdom is related to rms through $\delta\mu_{\rm sdom} = \delta\mu_{\rm rms}/\sqrt{N_{\rm tg}}$. Both $\delta\mu_{\rm rms}$ and $\delta\mu_{\rm sdom}$ are determined by the dispersion of TG rates around their average, and are independent on uncertainties δr_i affecting the individual rates r_i. Therefore, it may be convenient (see e.g. Mitrovica *et al.* 2001) to introduce a weighted rms, or wrms:

$$\delta\mu_{\rm wrms} = \sqrt{\frac{\sum_{i=1}^{N_{\rm tg}} w_i\,(r_i - \mu)^2}{\sum_{i=1}^{N_{\rm tg}} w_i}}, \tag{6}$$

where $w_i = (\delta r_i)^{-2}$. In what follows, estimates of uncertainty on μ will be given as $\delta\mu = \delta\mu_{\rm rms}$, but for the sake of completeness we will give also a numerical value for $\delta\mu_{\rm wrms}$. Using values listed in Table 2 of Spada & Galassi (2012) into eqs (4)–(6), the rate of GMSLR is

$$\mu \pm \delta\mu = (1.58 \pm 0.38)\ \text{mm yr}^{-1} \quad (1\sigma,\ \delta\mu_{\rm wrms} = 0.36\ \text{mm yr}^{-1}). \tag{7}$$

Similarly, the average contribution of GIA on $\dot{S}$ at TGs is

$$\gamma = \frac{1}{N_{\rm tg}} \sum_{i=1}^{N_{\rm tg}} g_i, \tag{8}$$

where g_i ($i = 1, \ldots, N_{\rm tg}$) are the rates of relative sea level change evaluated as an average over the models that, in the ensemble, are equivalent to the nominal ICE-3G(VM1). In analogy with μ, two measures of uncertainty can be computed for γ. These are the rms

$$\delta\gamma = \delta\gamma_{\rm rms} = \sqrt{\frac{\sum_{i=1}^{N_{\rm tg}} (g_i - \gamma)^2}{N_{\rm tg} - 1}}, \tag{9}$$

and the weighted rms

$$\delta\gamma_{\rm wrms} = \sqrt{\frac{\sum_{i=1}^{N_{\rm tg}} w_i\,(g_i - \gamma)^2}{\sum_{i=1}^{N_{\rm tg}} w_i}}, \tag{10}$$

where the weights $w_i = (\delta g_i)^{-2}$ are determined by the T1 uncertainties on g_i. Using the GIA corrections shown in Fig. 3(c), eqs (8)–(10)

give

$$\gamma \pm \delta\gamma = (-0.18 \pm 0.19)\,\mathrm{mm\ yr^{-1}} \quad (1\sigma,\ \delta\gamma_{\mathrm{wrms}} = 0.13\,\mathrm{mm\ yr^{-1}}). \tag{11}$$

Hence, combining the uncertainties on μ and γ in quadrature and keeping only one significant decimal place as it is customarily done in sea level rise studies (see Table 1 of Spada & Galassi 2012), we obtain the GIA-corrected rate of secular sea level rise:

$$\rho = (\mu - \gamma) \pm \sqrt{(\delta\mu)^2 + (\delta\gamma)^2} = (1.8 \pm 0.4)\,\mathrm{mm\ yr^{-1}} \quad (1\sigma,\ \delta\rho_{\mathrm{wrms}} = 0.4\,\mathrm{mm\ yr^{-1}}). \tag{12}$$

We note that the T1 uncertainty on ρ would not significantly change (at the 0.1 mm yr^{-1} level) neglecting $\delta\gamma$ in front of $\delta\mu$ [*i.e.* assuming that ICE-3G(VM1) is immune from imperfections]. This result holds both for the rms and wrms measures of uncertainty. Thus, the GMSLR uncertainty in eq. (12), *i.e.* 0.4 mm yr^{-1}, essentially originates from the TG data, and not from T1 GIA uncertainties despite their importance at a few specific locations in the neighbours of previously glaciated regions (see Fig. 3c).

5.3 Absolute sea level, altimetry observations and gravity variations

Similar to TG data, rates of absolute sea level change observed from altimetry require a GIA correction to enlighten the present-day climate change contribution. However, since altimeters are directly sampling the oceans surface, the appropriate correction is not $\dot{S}$, but the rate of sea surface variation $\dot{N}$ (see e.g. Tamisiea 2011). Furthermore, altimetry observations are expected to be not affected by the bias of TG observations, caused by their poor geographical coverage. In Fig. 4(a), the $\dot{N}$ fingerprint is shown for the nominal ICE-3G(VM1); Fig. 4(b) shows its 1σ T1 uncertainty $\Delta\dot{N}$. By the SLE (eq. 1), the VLM fingerprint would be given by $\dot{U} = \dot{N} - \dot{S}$, where $\dot{S}$ is shown in Fig. 3(a). In our GIA computations, consistently with the conventions used in altimetry, $\dot{N}$ is evaluated in the reference frame with origin coincident with the centre of mass of the whole Earth system, including the solid component and the fluid parts. Since the GIA contribution to $\dot{N}$ varies smoothly across the oceans, a common practice is to correct the rates observed by altimetry by subtracting the ocean-average $<\dot{N}>$, which according to calculations based on various GIA models turns out to be close to -0.3 mm yr^{-1} (Church *et al.* 2013; WCRP 2018). Hence, while on average GIA is causing a collapse of the sea surface relative to the geocentre, the average sea surface is not moving with respect to the oceans bottom, according to eq. (3).

Despite the small value of $\langle\dot{N}\rangle$ compared to the rate of absolute sea level change observed during the 'altimetry era' (1992–today, $\sim$3.5 mm yr^{-1}, see Church *et al.* 2013), estimating its modelling uncertainty may be of some interest. From our Monte Carlo simulation, we find

$$\langle\dot{N}(\omega)\rangle = (-0.30 \pm 0.06) \quad \mathrm{mm\ yr^{-1}} \quad (1\sigma), \tag{13}$$

a value in fair agreement with predictions from state-of-the-art GIA models (e.g. Church *et al.* 2013; Spada 2017). Result (13) shows that T1 uncertainties on $\langle\dot{N}\rangle$ are significant, in relative terms (20 per cent). We remark that eq. (13) provides a tighter constraint on the possible range of $\langle\dot{N}\rangle$ in comparison with that determined by Tamisiea (2011), who varied the Earth's rheological profile within plausible ranges, but did not impose the fit so obtained with a global set of Holocene RSL data, as we have done here.

The field N is related to the total geopotential variation Φ by

$$N(\omega, t) = \frac{\Phi}{\overline{g}} + c, \tag{14}$$

where $\overline{g}$ is the reference gravity at the Earth's surface and $c(t)$ is the spatially invariant constant introduced by Farrell & Clark (1976) to ensure mass conservation in GIA modelling (see also Tamisiea 2011; Spada 2017). Hence, for harmonic degrees $l \geq 2$ and orders $0 \leq m \leq l$, the GIA-induced rate of change of the fully normalized cosine and sine Stokes coefficients is

$$\dot{c}_{lm} + i\dot{s}_{lm} = (-1)^m \sqrt{2 - \delta_{0m}}\ \frac{\dot{N}^*_{lm}}{a}, \tag{15}$$

where we have used the definition of Stokes coefficients (e.g. Heiskanen & Moritz 1981); we have adopted the GRACE normalization conventions for spherical harmonics[3] (Bettadpur 2018), a is the average Earth's radius, $\dot{N}_{lm}$ are the coefficients of the complex 4π-normalized spherical harmonic expansion of $\dot{N}$, and $i = \sqrt{-1}$ (Spada & Stocchi 2006). Because the origin of the GIA reference frame has been chosen to be coincident with the centre of mass of the whole Earth, the variations in the Stokes coefficients in eq. (15) vanish for harmonic degree $l = 1$, in agreement with satellite geodetic convention (e.g. Bettadpur 2018). Since the time variations of the Stokes coefficients are observed by the GRACE satellite (e.g. Wahr *et al.* 1998), it is of some interest to consider their T1 GIA uncertainties using eq. (15). We prefer not to express our results in terms of equivalent water thickness since for non-surficial processes such as GIA it has been shown that this practice leads to misinterpretations (Chao 2016). As shown in Fig. 4(c), the T1 GIA uncertainties on $\dot{c}_{lm}$ and $\dot{s}_{lm}$ vary with l and m in a quite complex way, although they have the general tendency to decrease with increasing degree (*i.e.* decreasing wavelength $\lambda \sim 2\pi a/l$). For the lowest degree coefficient, associated with changes in the Earth's oblateness, we find

$$\dot{c}_{20} = (1.94 \pm 0.53) \times 10^{-11}\ \mathrm{yr^{-1}} \quad (1\sigma). \tag{16}$$

Thus, for this coefficient, the GIA relative uncertainty ($\sim$ 25 per cent) is remarkable, largely exceeding the one typically associated with, for example, satellite laser ranging measurements ($\sim$ 10 per cent; see e.g. Cheng *et al.* 1989). This result is clearly a consequence of the strong zonal pattern shown by $\Delta\dot{N}$ in Fig. 4(b).

6 GUESSING THE T2 UNCERTAINTIES

A reliable estimate of the T2 uncertainty, associated with structural differences in GIA models, is obviously hampered by the limited number of samples (*i.e.* state-of-the-art global models) existing and publicly available. Hence, aware of the sketchy character of the ensuing discussion, we consider two state-of-the-art GIA models, namely, ICE-6G_C(VM5a) of Peltier *et al.* (2015) and the one progressively developed at the Australian National University by Kurt Lambeck and collaborators, hereafter referred to as ANU (see e.g. Nakada & Lambeck 1987; Lambeck *et al.* 2003). For ICE-6G_C(VM5a), the chronology of melting is available from the web page of WR Peltier[4], while for ANU the data have been kindly provided to GS by Anthony Purcell on November 2016. This version

[3] See ftp://podaac.jpl.nasa.gov/allData/grace/docs/L2-UserHandbook_v4.0.pdf (last visited on 2018 December 12).

[4] See http://www.atmosp.physics.utoronto.ca/~peltier/data.php (last visited 2019 March 15).

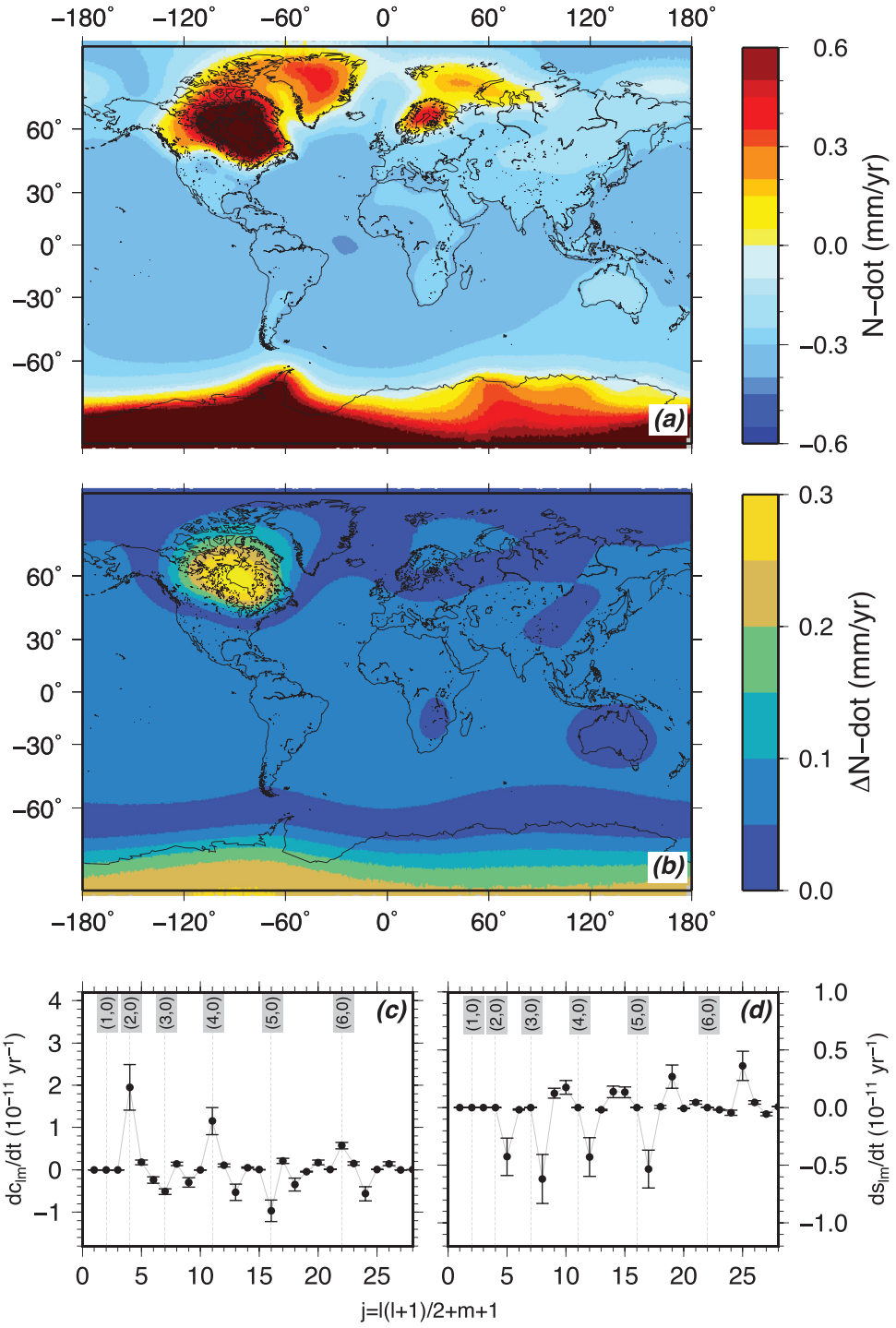

Figure 4. $\dot{N}$ fingerprint (a) for the nominal ICE-3G(VM1) model and its 1σ T1 uncertainty $\Delta\dot{N}$ (b). Predicted present-day rates of change of the cosine and sine Stokes coefficients for harmonic degrees $2 \leq l \leq 6$ and orders $0 \leq m \leq l$ coefficients are shown in (c) and (d), respectively. For ease of viewing, the colour scales in (a) and (b) are saturated.

of the ANU model has been upgraded and published by Lambeck *et al.* (2017) shortly after (Anthony Purcell, personal communication, 2016). These two recent and independently developed models are constrained by distinct global sets of RSL data and geodetic observations. Furthermore, since their deglaciation histories are available, they can be implemented in an independently developed SLE solver to facilitate the models intercomparison. With the aim of assessing the GIA modelling uncertainty in the context of global climate change, this same mini-ensemble approach has been taken by the IPCC AR5 (Church *et al.* 2013), based, however, on previous versions of the two models and limited to the rate of relative sea level change[5]. A different perspective has been adopted by Huang

[5]See ftp://ftp-icdc.cen.uni-hamburg.de/ar5_sea_level_rise/ (last visited on 2019 March 13).

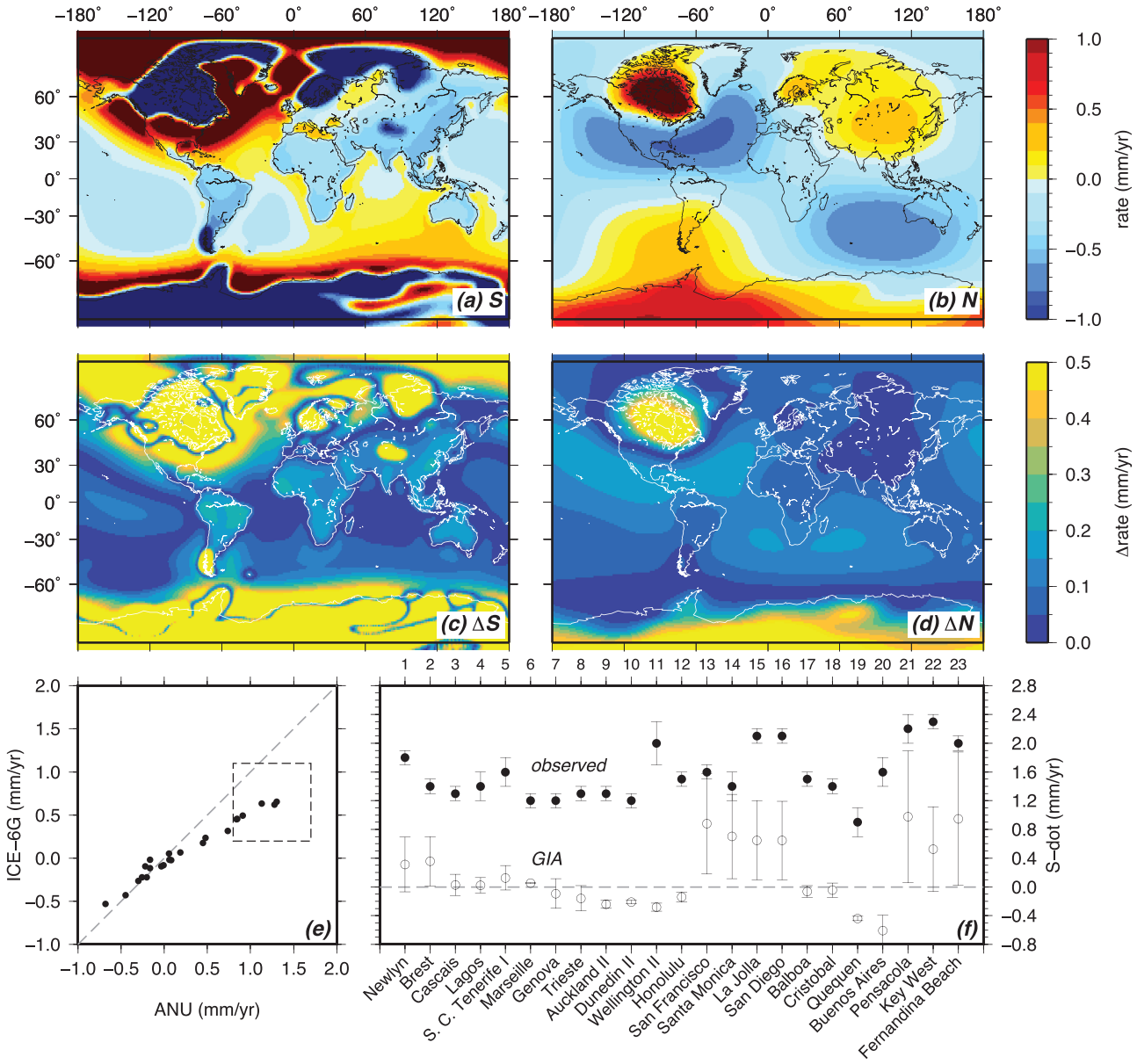

Figure 5. Mini-ensemble present-day rates of relative sea level change ($\dot{S}$, a), of absolute sea level change ($\dot{N}$, b), and their 1σ T2 uncertainties $\Delta\dot{S}$ (c) and $\Delta\dot{N}$ (d). GIA predictions obtained from the two models at the 23 Douglas (1997) TGs are compared in (e), while in (f) we compare ensemble GIA predictions for $\dot{S}$ (with T2 uncertainties) with observations. For ease of viewing, the uncertainties shown in (f) correspond to 2σ, while the colour scales in (a)–(d) are saturated.

(2013), who following the previous work by Guo *et al.* (2012) considered about 10 historically developed GIA models. However, some of them are not independent, and some are characterized by intrinsic limitations such as the lack of rotational feedback or the use of outdated ice models. Thus, such approach would not fit our concept of T2 uncertainty, which involves the use of state-of-the-art and independently developed models, characterized by all the essential features that ensure a realistic description of GIA.

For both ICE-6G_C(VM5a) and ANU models, we have numerically solved a generalized gravitationally and topographically self-consistent SLE (eq. 1), in which we account for the horizontal migration of shorelines and for the transition between grounded and floating ice. A module for computing the effects of the rotational feedback on sea level has been also implemented, following the revised rotational theory of Mitrovica *et al.* (2005) and Mitrovica & Wahr (2011), which extends the previous work of Milne & Mitrovica (1998). The adopted GIA theory, which is based on the results of Mitrovica & Milne (2003), has been implemented into the program SELEN4, which improves upon the SLE solver SELEN originally introduced by Spada & Stocchi (2007), only suitable for the classical Farrell & Clark (1976) theory. SELEN4 has been recently successfully benchmarked against independently developed SLE solvers (Martinec *et al.* 2018). For both models, we have assumed incompressibility and employed a nine-layer mantle with a linear Maxwell rheology and a density profile based on the PREM model of Dziewonski & Anderson (1981), assuming a perfectly elastic lithosphere. For model ICE-6G_C(VM5a), we have adopted the viscosity profile presented in the supporting information of Peltier

et al. (2015). For ANU, we have adopted a lithospheric thickness of 90 km, an upper-mantle viscosity of 0.5×10^{21} Pa s, and a lower mantle viscosity of 10^{22} Pa s, falling within the range of parameters suggested by Lambeck *et al.* (2017).

Figs 5(a) and (b) show the ensemble-averaged $\dot{S}$ and $\dot{N}$ fields, respectively. The effects of Earth rotation are now evident on $\dot{N}$, showing a clear degree $l = 2$ and order $m = 1$ lobed pattern; the $\dot{S}$ field shows a comparatively stronger regional variability, caused by the GIA-induced VLM. The T2 uncertainties $\Delta\dot{S}$ and $\Delta\dot{N}$ are shown in Figs 5(c) and (d), respectively. Following the GIA mini-ensemble approach taken by the IPCC AR5 (Church *et al.* 2013), the T2 uncertainties have been evaluated as the sample standard deviation of the fields computed using ICE-6G_C(VM5a) and ANU, which correspond, at the 1σ level, to the absolute difference of the two fields divided by $\sqrt{2}$. Similar to their T1 counterparts in Figs 3 and 4, the T2 uncertainties are characterized by a strong zonal pattern with peak values across the previously glaciated areas and the surrounding collapsing forebulges. The maximum amplitudes found here ($\sim$9.6 mm yr^{-1} for $\Delta\dot{S}$ and $\sim$0.8 mm yr^{-1} for $\Delta\dot{N}$, respectively) largely exceed the typical T1 values (see Fig. 3). In the equatorial regions, $\Delta\dot{S}$ and $\Delta\dot{N}$ generally do not exceed the $\sim$0.1 mm yr^{-1} level; in particular, from Fig. 5(d) we note that $\Delta\dot{N}$ is generally characterized by a rather modest variability across the oceans.

Predictions of the two models at the Douglas (1997) TGs, shown in the scatterplot of Fig. 5(e), are generally consistent to within a few tenths of mm yr^{-1}. However, differences are apparent for the sites corresponding to the points in the box, located along the North American West Coast and in South East North America, where the ANU rates neatly exceed the ICE-6G_C(VM5a) rates. This may reflect structural differences in the time history and geometry of the Laurentian ice sheet in the two GIA models, but also the relatively large viscosity increase that ANU assumes in the lower mantle, causing a delayed response to unloading relative to ICE-6G_C(VM5a), hence a larger isostatic disequilibrium at present time (see also discussion in Spada & Galassi 2012). In relative terms, the impact on the T2 uncertainties in Fig. 5(f) is significant, ranging between 40 per cent and 60 per cent for TGs along the North American West Coast and in South East North America, comparable to that obtained for T1 in Fig. 3(c), where the GIA correction is significant.

Following the same procedure outlined in Section 5.2, we have employed the results in Fig. 5(f) to estimate the (GIA-corrected) GMSLR, obtaining $\rho = (1.4 \pm 0.6)$ mm yr^{-1} (1σ, $\delta\rho_{\rm wrms} = 0.4$ mm yr^{-1}). In this case, we have found that T2 is affecting the GMSLR rms uncertainty at the 0.2 mm yr^{-1} level, that is, only about one-third of the total uncertainty, dominated by the dispersion of the sea level trend at TGs. Conversely, at the 0.1 mm yr^{-1} level, the wrms uncertainty originates from the intrinsic variability of TG time-series. The smaller amount of GMSLR compared to eq. (12) is consistent with findings based on previous versions of the two models considered here (Spada & Galassi 2012) and with the recent probabilistic assessment of Hay *et al.* (2015). Lastly, we have considered the T2 uncertainty on the ocean-averaged rate of absolute sea level change and on the rate of change of the Stokes coefficient c_{20}. For the former, we obtain $\dot{\mathcal{V}} = (-0.3 \pm 0.1)$ mm yr^{-1} (1σ), while for the latter we get $\dot{c}_{20} = (2.3 \pm 1.0) \times 10^{-11}$ yr^{-1} (1σ). Although having a different meaning, these estimates are substantially consistent with our findings about the T1 uncertainties in Section 5. Even if based on a very limited set of GIA models (two), our results on the large uncertainty on the GIA contribution to the $\dot{c}_{20}$ Stokes coefficient essentially confirm the recent findings of Caron *et al.* (2018), and indicates the need of further refinements in GIA modelling. We attribute this large uncertainty to the difference in the lower mantle viscosity for the two models included in our mini-ensemble.

7 CONCLUSIONS

Using a suite of GIA models that describe the delayed response of the Earth to the melting of late-Pleistocene ice sheets, we have shown that it is possible to define two sources of uncertainty. These two types of uncertainty, while not strictly independent of each other, stem from different aspects of imperfect knowledge. The first (T1) has been evaluated considering a large ensemble of models with distinct input parameters (e.g. the viscosity profiles) and regional distributions of ice volumes, constrained by a unique RSL data set and by the same eustatic curve. The second (T2) accounts, in addition to differences in input parameters, for more structural differences in two state-of-the-art, independently developed GIA models. Our computations, although not exhaustive, have shown that *input uncertainties* (T1) are comparable with *structural uncertainties* (T2) for a range of GIA-related geophysical quantities and both substantially contribute to the overall uncertainty in GIA modelling. However, T1 and T2 are affecting the GIA fingerprints in different manners at regional and global scales. In particular, at TGs in the periphery of formerly ice-covered regions, both types of uncertainty on the GIA-modelled rates of sea level change till now exceed those on the observed trends. Nevertheless, we have found that the uncertainty on GMSLR is only marginally affected by the GIA modelling uncertainties, being dominated by the dispersion of the observed TG rates. This result is quite robust since it holds for both types of uncertainties considered in this study. GIA corrections on the ocean-averaged absolute sea level change are small compared to the rates observed by satellite altimetry. However, we have found that they are significantly affected by T1 modelling uncertainties in GIA, and the same holds for the time variations of the long-wavelength Stokes coefficients of the Earth's gravity field, in agreement with recent independent findings by Caron *et al.* (2018).

This study supports the idea that quantifying GIA uncertainties is extremely important for understanding changes in the climate system (Tamisiea 2011; Spada 2017; Whitehouse 2018) and in particular to verify the closure of the sea level budget during the altimetry era (WCRP 2018). However, at present, a rigorous assessment of the size of the T2 uncertainties is hindered by the very limited number of independently developed global GIA models available and testable. The increasing quality of geodetic data and modelling efforts along the lines outlined above and in other studies (e.g. Caron *et al.* 2018), either based on traditional spherically symmetric models or on a more realistic 3D rheology, are expected to significantly refine current estimates of GIA modelling uncertainties.

ACKNOWLEDGEMENTS

We thank Lambert Caron and Patrick Wu for providing a number of very valuable suggestions and constructive comments, which have helped considerably to improve the manuscript. We also thank Anthony Purcell for having made the ANU model data available to us and Richard Peltier for distributing the ice sheets chronology of ICE-6G_C(VM5a) online. All the figures have been drawn using the Generic Mapping Tools of Wessel & Smith (1998). The open-source program SELEN is available from the Computational Infrastructure for Geodynamics, at the address

http://geodynamics.org/cig/software/selen/. All the data and procedures employed in this study are available from the authors under request. To facilitate reproducibility of our results, time frames of the ice thickness time history are, in particular, also available from the authors. GS is funded by an FFABR (Finanziamento delle Attività Base di Ricerca) grant of the MIUR (Ministero dell'Istruzione, dell'Università e della Ricerca) and by a DiSPeA (Dipartimento di Scienze Pure e Applicate of the Urbino University) research grant. This work is partly funded by the PNRA (Programma Nazionale di Ricerche in Antartide). We are indebted to Erika Pigliapoco for providing invaluable support.

REFERENCES

Bettadpur, S., 2018. *Level-2 gravity field product user handbook,* Revision 4.0, GRACE 327-734, The GRACE Project, Jet Propulsion Laboratory.

Caron, L., Métivier, L., Greff-Lefftz, M., Fleitout, L. & Rouby, H., 2017. Inverting Glacial Isostatic Adjustment signal using Bayesian framework and two linearly relaxing rheologies, *Geophys. J. Int.*, **209**(2), 1126–1147.

Caron, L., Ivins, E., Larour, E., Adhikari, S., Nilsson, J. & Blewitt, G., 2018. GIA model statistics for GRACE hydrology, cryosphere, and ocean science, *Geophys. Res. Lett.*, **45**(5), 2203–2212.

Chao, B., 2016. Caveats on the equivalent water thickness and surface mascon solutions derived from the GRACE satellite-observed time-variable gravity, *J. Geod.,* **90**(9), 807–813.

Cheng, M., Eanes, R., Shum, C., Schutz, B. & Tapley, B., 1989. Temporal variations in low degree zonal harmonics from Starlette orbit analysis, *Geophys. Res. Lett.*, **16**(5), 393–396.

Church, J. *et al.*, 2013. Sea level change, in *Climate Change 2013: The Physical Science Basis. Contribution of Working Group I to the Fifth Assessment Report of the Intergovernmental Panel on Climate Change,* pp. 1138–1191, eds Stocker, T., Qin, D. , Tignor, M., Allen, S., Boschung, J., Nauels, A., Xia, Y., Bex, V., Midgley, P. *et al.*, Cambridge Univ. Press.

Douglas, B., 1997. Global sea leve rise: a redetermination, *Surv. Geophys.,* **18,** 279–292.

Dziewonski, A.M. & Anderson, D.L., 1981. Preliminary reference Earth model, *Phys. Earth planet. Inter.*, **25**(4), 297–356.

Engelhart, S., Peltier, W. & Horton, B., 2011. Holocene relative sea level changes and glacial isostatic adjustment of the U.S. Atlantic coast, *Geology,* **39,** 751–754.

Farrell, W. & Clark, J., 1976. On postglacial sea level, *Geophys. J. R. astr. Soc.*, **46,** 647–667.

Guo, J., Huang, Z., Shum, C. & van der Wal, W., 2012. Comparisons among contemporary glacial isostatic adjustment models, *J. Geodyn.*, **61,** 129–137.

Hay, C.C., Morrow, E., Kopp, R.E. & Mitrovica, J.X., 2015. Probabilistic reanalysis of twentieth-century sea level rise, *Nature,* **517**(7535), 481–484.

Heiskanen, W.A. & Moritz, H., 1981. *Physical Geodesy,* Institute of Physical Geodesy, Technical University.

Huang, Z., 2013. *The Role of Glacial Isostatic Adjustment (GIA) Process on the Determination of Present-Day Sea level Rise,* The Ohio State University.

Jevrejeva, S., Moore, J., Grinsted, A., Matthews, A. & Spada, G., 2014. Trends and acceleration in global and regional sea levels since 1807, *Glob. Planet. Change,* **113,** 11–22.

Kennedy, M.C. & O'Hagan, A., 2001. Bayesian calibration of computer models, *J. R. Stat. Soc. B,* **63**(3), 425–464.

King, M.A. *et al.*, 2010. Improved constraints on models of glacial isostatic adjustment: a review of the contribution of ground-based geodetic observations, *Surv. Geophys.,* **31**(5), 465–507.

Kotz, S., Balakrishnan, N. & Johnson, N.L., 2004. *Continuous Multivariate Distributions, Models and Applications,* Vol. 1, John Wiley & Sons.

Lambeck, K., Smither, C. & Johnston, P., 1998. Sea level change, glacial rebound and mantle viscosity for northern Europe, *Geophys. J. Int.*, **134**(1), 102–144.

Lambeck, K., Purcell, A., Johnston, P., Nakada, M. & Yokoyama, Y., 2003. Water-load definition in the glacio-hydro-isostatic sea level equation, *Quat. Sci. Rev.,* **22**(2), 309–318.

Lambeck, K., Rouby, H., Purcell, A., Sun, Y. & Sambridge, M., 2014. Sea level and global ice volumes from the Last Glacial Maximum to the Holocene, *Proc. Natl. Acad. Sci.,* **111**(43), 15 296–15 303.

Lambeck, K., Purcell, A. & Zhao, S., 2017. The North American Late Wisconsin ice sheet and mantle viscosity from glacial rebound analyses, *Quat. Sci. Rev.,* **158,** 172–210.

Martinec, Z. *et al.*, 2018. A benchmark study of numerical implementations of the sea level equation in GIA modelling, *Geophys. J. Int.*, **215**(1), 389–414.

Milne, G.A. & Mitrovica, J.X., 1998. Postglacial sea level change on a rotating Earth, *Geophys. J. Int.*, **133**(1), 1–19.

Mitrovica, J.X. & Milne, G.A., 2002. On the origin of late Holocene sea level highstands within equatorial ocean basins, *Quat. Sci. Rev.,* **21**(20), 2179–2190.

Mitrovica, J.X. & Milne, G.A., 2003. On post-glacial sea level: I. General theory, *Geophys. J. Int.*, **154**(2), 253–267.

Mitrovica, J.X. & Wahr, J., 2011. Ice Age Earth Rotation, *Annu. Rev. Earth Planet. Sci.,* **39,** 577–616.

Mitrovica, J.X., Tamisiea, M.E., Davis, J.L. & Milne, G.A., 2001. Recent mass balance of polar ice sheets inferred from patterns of global sea level change, *Nature,* **409**(6823), 1026–1029.

Mitrovica, J.X., Wahr, J., Matsuyama, I. & Paulson, A., 2005. The rotational stability of an ice-age earth, *Geophys. J. Int.*, **161**(2), 491–506.

Nakada, M. & Lambeck, K., 1987. Glacial rebound and relative sea level variations: a new appraisal, *Geophys. J. Int.*, **90**(1), 171–224.

Peltier, W.R., 1994. Ice age paleotopography, *Science,* **265**(5169), 195–195.

Peltier, W.R., Argus, D.F. & Drummond, R., 2015. Space geodesy constrains ice age terminal deglaciation: the global ICE-6G_C (VM5a) model, *J. geophys. Res.,* **120**(1), 450–487.

Peltier, W.R., Argus, D.F. & Drummond, R., 2018. Comment on "An assessment of the ICE-6G_C (VM5a) Glacial Isostatic Adjustment Model" by Purcell et al., *J. geophys. Res.,* **123**(2), 2019–2028.

Pfeffer, J., Spada, G., Mémin, A., Boy, J.-P. & Allemand, P., 2017. Decoding the origins of vertical land motions observed today at coasts, *Geophys. J. Int.*, **210**(1), 148–165.

Plag, H.-P. & Jüettner, H.-U., 2001. Inversion of global tide gauge data for present-day ice load changes (scientific paper), *Mem. Natl. Inst. Polar Res.,* **54,** 301–317.

PSMSL, 2013. Permanent service for mean sea level, tide gauge data, Available at: http://www.psmsl.org/obtaing, (last accessed: 2013 July 2).

Purcell, A., Tregoning, P. & Dehecq, A., 2016. An assessment of the ICE6G_C (VM5a) glacial isostatic adjustment model, *J. geophys. Res.,* **121**(5), 3939–3950.

Santamaría-Gómez, A., Gravelle, M., Dangendorf, S., Marcos, M., Spada, G. & Wöppelmann, G., 2017. Uncertainty of the 20th century sea level rise due to vertical land motion errors, *Earth planet. Sci. Lett.*, **473,** 24–32.

Serpelloni, E., Faccenna, C., Spada, G., Dong, D. & Williams, S.D., 2013. Vertical GPS ground motion rates in the Euro-Mediterranean region: new evidence of velocity gradients at different spatial scales along the Nubia-Eurasia plate boundary, *J. geophys. Res.,* **118**(11), 6003–6024.

Simon, K., James, T., Henton, J. & Dyke, A., 2016. A glacial isostatic adjustment model for the central and northern Laurentide Ice Sheet based on relative sea level and GPS measurements, *Geophys. J. Int.*, **205**(3), 1618–1636.

Spada, G., 2017. Glacial isostatic adjustment and contemporary sea level rise: an overview, *Surv. Geophys.,* **38**(1), 1–33.

Spada, G. & Galassi, G., 2012. New estimates of secular sea level rise from tide gauge data and GIA modelling, *Geophys. J. Int.*, **191**(3), 1067–1094.

Spada, G. & Galassi, G., 2017. Extent and dynamic evolution of the lost land *aquaterra* since the Last Glacial Maximum, *C. R. Geosci.,* **349**(4), 151–158.

Spada, G. & Stocchi, P., 2006. *The Sea Level Equation, Theory and Numerical Examples,* Aracne.

Spada, G. & Stocchi, P., 2007. SELEN: a Fortran 90 program for solving the "Sea Level Equation", *Comput. Geosci.*, **33**(4), 538–562.

Spada, G. *et al.*, 2011. A benchmark study for glacial isostatic adjustment codes, *Geophys. J. Int.*, **185**(1), 106–132.

Steffen, H., Kaufmann, G. & Lampe, R., 2014. Lithosphere and upper-mantle structure of the southern Baltic Sea estimated from modelling relative sea level data with glacial isostatic adjustment, *Solid Earth,* **5**(1), 447–459.

Stocchi, P. & Spada, G., 2009. Influence of glacial isostatic adjustment upon current sea level variations in the Mediterranean, *Tectonophysics,* **474**(1), 56–68.

Sturges, W. & Hong, B., 2001. Decadal variability of sea level, in *Sea Level Rise: History and Consequences,* International Geophysics, Vol. **75,** pp. 165–180, eds Douglas, B.C., Kearney, M.S. & Leatherman, S.P., Elsevier.

Sørensen, P.B., Carlsen, L., Fauser, P. & Vikelsøe, J., 2001. Paradigm for analysing complex model uncertainty: a general concept for dealing with uncertainties in ecotoxicological models. Miljøkemi-environmental chemistry, Tech. Rep., National Environmental Research Institute.

Tamisiea, M.E., 2011. Ongoing glacial isostatic contributions to observations of sea level change, *Geophys. J. Int.*, **186**(3), 1036–1044.

Tushingham, A. & Peltier, W., 1991. ICE-3G – a new global model of late Pleistocene deglaciation based upon geophysical predictions of post-glacial relative sea level change, *J. geophys. Res.*, **96**(B3), 4497–4523.

Tushingham, A. & Peltier, W., 1992. Validation of the ICE-3G model of Würm-Wisconsin deglaciation using a global data base of relative sea level histories, *J. geophys. Res.*, **97**(B3), 3285–3304.

Tushingham, A. & Peltier, W., 1993. Relative Sea Level Database. IGPB PAGES/World Data Center-A for Paleoclimatology Data Contribution Series, Tech. Rep., 93–106.

Vacchi, M., Marriner, N., Morhange, C., Spada, G., Fontana, A. & Rovere, A., 2016. Multiproxy assessment of Holocene relative sea level changes in the western Mediterranean: sea level variability and improvements in the definition of the isostatic signal, *Earth-Sci. Rev.,* **155,** 172–197.

Wahr, J., Molenaar, M. & Bryan, F., 1998. Time variability of the Earth's gravity field: hydrological and oceanic effects and their possible detection using GRACE, *J. geophys. Res.,* **103**(B12), 30 205–30 229.

WCRP, 2018. Global Sea Level Budget 1993–Present, *Earth Syst. Sci. Data,* **10,** 1551–1590.

Wessel, P. & Smith, W.H.F., 1998. New, improved version of generic mapping tools released, *EOS, Trans. Am. geophys. Un.,* **79**(47), 579, doi:10.1029/98EO00426.

Whitehouse, P., 2009. Glacial isostatic adjustment and sea level change, State of the art Rep, Svensk Kärnbränslehantering AB, Swedish Nuclear Fuel and Waste Management Co., 105.

Whitehouse, P.L., 2018. Glacial isostatic adjustment modelling: historical perspectives, recent advances, and future directions, *Earth Surf. Dyn.,* **6**(2), 401–429.

Wöppelmann, G. & Marcos, M., 2016. Vertical land motion as a key to understanding sea level change and variability, *Rev. Geophys.,* **54**(1), 64–92.

Wu, P. & Peltier, W., 1982. Viscous gravitational relaxation, *Geophys. J. Int.*, **70**(2), 435–485.